

# VLBI imaging of OH absorption: The puzzle of the nuclear region of NGC 3079

Yoshiaki Hagiwara,<sup>1\*</sup> Hans-Rainer Klöckner,<sup>2,1</sup> Willem Baan<sup>1</sup>

<sup>1</sup>*ASTRON, Westerbork Observatory, P.O. Box 2, Dwingeloo, 7990 AA, The Netherlands*

<sup>2</sup>*Kapteyn Astronomical Institute, University of Groningen, Postbus 800, Groningen, The Netherlands*

2003

## ABSTRACT

Broad hydroxyl (OH) absorption-lines in the 1667 MHz and 1665 MHz transition towards the central region of NGC 3079 have been observed at high resolution with the European VLBI Network (EVN). Velocity fields of two OH absorption components were resolved across the unresolved nuclear radio continuum of  $\sim 10$  parsecs. The velocity field of the OH absorption close to the systemic velocity shows rotation in nearly the same sense as the edge-on galactic-scale molecular disk probed by CO(1–0) emission. The velocity field of the blue-shifted OH absorption displays a gradient in almost the opposite direction. The blue-shifted velocity field represents a non-rotational component, which may trace an outflow from the nucleus, or material driven and shocked by the kiloparsec-scale superbubble. This OH absorption component traces a structure that does not support a counter-rotating disk suggested on the basis of the neutral hydrogen absorption.

**Key words:** galaxies: active – galaxies:individual (NGC 3079): ISM – galaxies: Seyfert – radio lines: galaxies

## 1 INTRODUCTION

NGC 3079 is an edge-on Sc galaxy housing a LINER (Low Ionisation Narrow Emission Line Region) nucleus (Heckman 1980) with a long history of observations at various wavelengths. The nucleus is also classified as a type 2 Seyfert nucleus (Ford et al. 1986). The galaxy has a systemic velocity of  $1116 \text{ km s}^{-1}$  (Irwin & Seaquist 1991), which gives the distance of 16 Mpc and hence 1 milliarcsec (mas) corresponds to approximately 0.08 pc, adopting  $H_0 = 75 \text{ km s}^{-1} \text{ Mpc}^{-1}$ . Observations of optical emissions with the Hubble Space Telescope (HST) have shown a number of outflowing filaments in a ‘superbubble’, produced by a combination of stellar winds and supernova explosions in a site of massive star formation. X-ray observations with Chandra show a clear correspondence of H $\alpha$ -line filaments with those in X-rays at the distance of  $\sim 65$  pc from the nucleus (Cecil et al. 2002). Throughout several X-ray observations, a highly obscured active galactic nucleus (AGN) and iron line emission towards the nucleus were found (Cecil et al. 2002). The center of the galaxy has been resolved by radio interferometry and reveals a double radio lobe extending 1.5 kpc on either side of the major axis of the galaxy and a puzzling nuclear structure on parsec scales (Irwin & Seaquist 1988). Due to the complexity of the radio structure, the interpretation of

the location of a true nucleus is not straightforward.

Broad ( $200\text{--}400 \text{ km s}^{-1}$ ) and deep ( $\tau \sim 0.5$ ) neutral hydrogen HI absorption and weaker but equally broad and deep OH absorption are found towards those compact radio sources in the nucleus. These absorptions have been studied in detail at various angular resolutions by radio interferometers. Based on the Very Large Array (VLA) observations at 1 arcsec resolution, Baan & Irwin (1995) considered that the two components of HI and OH absorptions are associated with an obscuring torus in the nuclear region. Multi-Element Radio Linked Interferometer Network (MERLIN) observations at sub-arcsecond resolution resolved the rotation of the HI absorption (Pedlar et al. 1996) in the same sense as the rotational trend traced by HI emission and CO(1–0) emission on galactic scales (Irwin & Seaquist 1991; Irwin & Sofue 1992). According to Very Long Baseline Interferometry (VLBI) observations at an angular resolution of 10–15 mas, three HI absorption components viewed against the resolved double-peaked radio source appear to be evidence for counter rotation relative to the rotation in the outer galaxy (Sawada-Satoh et al. 2000).

The strong and highly intensity-variable water maser emission is known to exist in NGC 3079 (Henkel et al. 1984; Haschick & Baan 1985). Earlier attempts for resolving the maser emission have been made since the late 1980s using VLBI (Haschick et al. 1990). At present, it is understood that the H<sub>2</sub>O maser components are distributed

\* E-mail: hagiwara@astron.nl (YH)

**Table 1.** Properties of NGC 3079. Coordinates in this table were phase centre values used for the data correlation at JIVE. Velocity with respect to LSR for radio definition is adopted from Irwin & Seaquist (1991). Optical classification was made by Heckman (1980) and Ford et al. (1986). Radio flux densities were measured by the VLBA (Sawada-Satoh et al. 2000). Infra-red (IR) luminosity is from Baan (1989). X-ray luminosity is from Cecil et al. (2002). We assume that  $H_0 = 75 \text{ km s}^{-1} \text{ Mpc}^{-1}$ .

RA (J2000)	10 <sup>h</sup> 01 <sup>m</sup> 57.8050 <sup>s</sup>
Decl (J2000)	55°40′47.080″
Systemic Velocity (21-cm HI)	1116 ± 1 km s <sup>-1</sup>
Distance	16 Mpc
Inclination (optical)	84°
Optical class	LINER/Seyfert 2
F <sub>ν</sub> (1.4 GHz)	5.7 ± 1.7 mJy
(8.4 GHz)	14.2 ± 0.7 mJy
(15 GHz)	24.4 ± 0.6 mJy
(22 GHz)	12.1 ± 0.7 mJy
L <sub>IR</sub>	3 × 10 <sup>10</sup> erg s <sup>-1</sup>
L <sub>X-ray</sub> (0.1–6.5keV)	1.0 × 10 <sup>42</sup> erg s <sup>-1</sup>
L <sub>X-ray</sub> (Fe line;6.4keV)	3.3 × 10 <sup>41</sup> erg s <sup>-1</sup>

within an elongated (disk-like) structure within a few parsecs from the nucleus (Trotter et al. 1998). Most of the maser components detected with VLBI lie in a velocity range  $V_{\text{LSR}}$  (LSR refers Local Standard of Rest.) = 956–1190 km s<sup>-1</sup> and are not associated with any of the jet components (Trotter et al. 1998; Sawada-Satoh et al. 2000). They are distributed nearly north-to-south, and are aligned roughly with the molecular disk traced by CO(1–0) (Position Angle (P.A.) = 15°) with a radius of 750 pc (Irwin & Sofue 1992). Several new weak components were recently detected, which extend the velocity range to about  $V_{\text{LSR}} = 1350 \text{ km s}^{-1}$  (Hagiwara et al. 2002a). Given the velocity distribution of all the maser features observed to date, the maser spectrum shows a rough symmetry w.r.t the systemic velocity of the galaxy ( $V_{\text{LSR}} \simeq 1116 \text{ km s}^{-1}$ ) (Hagiwara et al. 2002b). It has been argued that there is a rotating parsec-scale molecular gas disk or torus obscuring an AGN in NGC 3079, but no concrete evidence has been presented in the literature like the one in NGC 4258 (Herrnstein et al. 1998). A recent study by Middelberg et al. (2003) presents evidence for five distinct radio continuum sources in the nucleus of NGC 3079, complicating the interpretation of its puzzling structure. Besides the three components A, B, and C that are detected at higher frequencies and are seen at 22 GHz together with the H<sub>2</sub>O masers, there are two other components E and F that are visible only at lower frequencies, following the convention used in Irwin & Seaquist (1988). These additional components have the same orientation and are equally spaced as the 22 GHz components A and B, but they are shifted about 25 mas  $\simeq 2 \text{ pc}$  to the east; they form the 18-cm radio signature that is observed in HI and OH absorption experiments.

In this paper, we present VLBI observations of OH absorption at the nuclear region of NGC 3079. With observations using European VLBI Network (EVN) at the highest spectral-line sensitivity of any existing VLBI facility, we aim to review the kinematics of the circumnuclear region in the galaxy.

## 2 OBSERVATIONS

The central region of NGC 3079 was observed at 18-cm on 2000 November 15 with the EVN, which consisted of eight telescopes: Cambridge, Effelsberg, Jodrell Bank (Lovell), Medicina, Noto, Onsala, Torun, and the Westerbork phased-array. We observed the 1667 and 1665 MHz main line transitions of the  $^2\Pi_{3/2}$ , J=3/2 ground-state of OH in absorption toward the central radio continuum source in NGC 3079.

NGC 3079 was observed in a phase-referencing mode over a period of 5.7 hrs, interspersed with observations of a phase calibrator source J0957+5522, which is located about 1 degree from the target source. The total time of one observing cycle was 13 minutes with 10 minutes for NGC 3079 and 3 minutes for J0957+5522. The total time spent on the target was about 3 hours. The data were recorded in both left and right circular polarizations using a single intermediate frequency (IF) band with 8 MHz bandwidth. The IF baseband was subdivided into 128 spectral points, yielding a frequency resolution of 62.5 kHz, or 11.2 km s<sup>-1</sup> in velocity at the source distance. The IF velocity coverage is 1440.5 km s<sup>-1</sup>. In order to cover both the main line transitions, we centered the IF on  $V_{\text{LSR}} = 1350 \text{ km s}^{-1}$  and the Doppler velocity center was referenced to the 1667 MHz line. Hereafter, all velocities are in the radio convention and with respect to LSR. The system temperature and antenna sensitivity for each EVN antenna over the observing frequency range from 30 K – 100 K during the observing run. DA 193 was measured in the middle of the observations for calibrating the absolute amplitude gain and the bandpass correction. The data-recording rate was 128 Mbit per second with a MkIV terminal.

The correlation of the data was performed at the EVN MkIV correlator at the Joint Institute for VLBI in Europe (JIVE). Data analysis was made using the NRAO AIPS package. After the delay and delay rate calibration using J0957+5522, the bandpass corrections were applied. We discarded the data from six baselines, Noto(NT)-Medicina(Mc), Mc-Torun(Tr), Tr-NT, Cambridge(Cm)-Tr, Cm-NT, and Cm-Mc baseline, due to inadequate data quality. The continuum visibility data set was generated from the spectral-line visibility data set by averaging absorption-free channels using the AIPS task of UVLIN. The continuum visibility data set was then used for self-calibration to improve the image sensitivity. After iterations of the self-calibration in both phase and amplitude, the solutions were transferred to the spectral-line visibility data. The continuum and spectral-line visibilities were imaged employing IMAGR.

## 3 RESULTS

Fig. 1 (*left*) shows the EVN spectrum of OH absorption integrated over the nuclear radio continuum source (Fig. 4) with natural weighting with a spectral resolution of 11.2 km s<sup>-1</sup>. The systemic velocity of the galaxy  $V_{\text{LSR}} = 1116 \text{ km s}^{-1}$  and the peak velocities of HI absorption and water maser emission are denoted. The rms noise level is 0.7 mJy beam<sup>-1</sup> per channel. The OH main-line transitions of 1667

MHz and 1665 MHz are clearly detected against an unresolved continuum source at the centre of NGC 3079. Both transitions have two distinct components, one of which is blue-shifted (OH1) and the other is nearly centred on the systemic velocity (OH2). This is consistent with the spectra at lower resolutions (Baan & Irwin 1995). By comparison with the single-dish spectrum, the OH absorption lines observed in these observations have lost their broad wings. The integrated intensities of the 1667 MHz OH absorption estimated from the single-dish and the EVN spectrum in Fig. 1 (*left*) are about  $8.3 \text{ Jy km s}^{-1}$  (Baan & Irwin 1995) and  $0.74 \text{ Jy km s}^{-1}$ , respectively. Only 8.9 percent of the absorption intensity was recovered in the EVN observations. This accounts for the narrower line-widths of the OH absorption spectra obtained with the EVN (Table 2). The OH emissions in the wing of the absorption at  $V_{\text{LSR}} = 910$  and around  $V_{\text{LSR}} = 1260 \text{ km s}^{-1}$  suggested by Baan & Irwin (1995) coincide with weak emission features seen in our EVN spectrum, although both of them need to be confirmed in further observations. Two Gaussian components have been fitted to the absorption profiles of each of the transition (Fig. 1 *right*); the results are listed in Table 2. The resultant opacity and column density are listed in Table 3 together with those of the previous VLA and VLBI observations obtained at different angular scales. The OH absorption velocity center (Gaussian-fitted) is  $V_{\text{LSR}}(\text{OH1}) = 1011.9 \pm 0.9 \text{ km s}^{-1}$  and  $V_{\text{LSR}}(\text{OH2}) = 1113.5 \pm 2.0 \text{ km s}^{-1}$ , while the centre velocities derived from the VLA-A data are  $V_{\text{LSR}} = 1013 \text{ km s}^{-1}$  and  $V_{\text{LSR}} = 1114 \text{ km s}^{-1}$  (Baan & Irwin 1995). These values are consistent within the spectral resolution of one channel. The HI absorptions are peaked at  $V_{\text{LSR}} = 1010 \text{ km s}^{-1}$ ,  $1120 \text{ km s}^{-1}$ , and  $1265 \text{ km s}^{-1}$  (Baan & Irwin 1995), where the red-shifted third component has no OH counterpart. The ratios of the double peaks in both transitions are quite consistent, which may imply that both main-line features are associated with the same continuum source. The line ratio 1667 to 1665 MHz in the Gaussian-fitted profiles is 1.5, which is lower than the Local Thermodynamic Equilibrium (LTE) value of 1.8.

Velocity-integrated maps of the 1667 MHz OH absorption integrated over  $11.2 \text{ km s}^{-1}$  intervals and the CLEAN map of a 18-cm radio continuum source are shown in Fig. 2 (All are uniformly weighted.). Fifteen velocity channel maps cover the velocity range of the absorption from  $990.4 \text{ km s}^{-1}$  to  $1147.7 \text{ km s}^{-1}$ .

The continuum emission was not resolved in this experiment. The peak flux density of the continuum map produced with uniform weighting is  $8.8 \text{ mJy beam}^{-1}$  and the rms noise level is  $0.25 \text{ mJy beam}^{-1}$ . The peak flux density and the noise level of the continuum map produced with natural weighting are  $11.8 \text{ mJy beam}^{-1}$  and  $0.085 \text{ mJy beam}^{-1}$ , respectively. The integrated flux density of the continuum is  $14.3 \pm 0.7 \text{ mJy}$ , while the 21-cm integrated flux density obtained by single-dish measurements is  $760 \pm 31 \text{ mJy}$  (Condon 1983). Hence, more than 95 percent of the continuum flux is missing in this EVN experiment. Because the limited angular resolution of our EVN observations compared with the past VLBI observations at higher frequencies, the nuclear continuum remains unresolved without showing any structure. The EVN synthesized beam is larger than the angular separation between the various nuclear components (Fig. 7), which limits the discussion on the possible associations of

the OH absorbing gas with individual sources in later sections.

A position-velocity (PV) diagram of the 1667 MHz absorption is presented in Fig. 3. A cut was made through the continuum emission at P.A. =  $15^\circ$  (rotated clockwise by 15 degrees), which aligns a cut along a major axis of the rotation traced by CO(1–0) (Sofue & Irwin 1992; Koda et al. 2002) and which was also used from the PV diagrams in Baan & Irwin (1995). The gradients in the 1665 MHz line show the same trend as those seen in the 1667 MHz line. Note that there are significant position offsets of  $\sim 7\text{--}8 \text{ mas}$  in declination between the two peaks of OH1 (blue-shifted) and OH2 (systemic), which could not be measured in the PV diagrams of Baan & Irwin (1995) at 1 arcsec resolution with the VLA-A. The velocity contours of OH1 and OH2 are separate, as compared with the PV diagrams in Fig. 7 in Baan & Irwin (1995).

Fig. 4 shows a naturally weighted 18-cm continuum map superposed on the integrated 1667 MHz OH intensity (0th moment) map. The absorption is apparently concentrated towards the centre with a weak outward extension. This is similar to the east-west elongation of the HI and OH absorbing gas seen at 1 arcsec resolution and caused by the orientation and separation ( $\sim 25 \text{ mas}$  or  $\sim 2 \text{ pc}$ ) of the L-band components E and F (Irwin & Seaquist 1988; Baan & Irwin 1995; Middelberg et al. 2003).

Fig. 5 displays the OH velocity field of the two components (1st moment). The velocity field of OH1 varies from southwest to northwest in P.A. =  $60^\circ$ , while that of OH2 is seen approximately from north to south in P.A. =  $145^\circ$ . The velocity gradients of OH1 and OH2 are  $\sim 10 \text{ km s}^{-1} \text{ pc}^{-1}$  and  $\sim 13 \text{ km s}^{-1} \text{ pc}^{-1}$ , respectively. The kpc-scale CO(1–0) velocity gradient is found to be also in the north-to-south direction and has a value of  $0.85 \text{ km s}^{-1} \text{ pc}^{-1}$  and a P.A. =  $15^\circ$  (Sofue & Irwin 1992). The compact nuclear CO(1–0) core at P.A. =  $4^\circ$ , tilted by about  $10^\circ$  w.r.t the kpc-scale CO(1–0) disk, within central 125 pc shows a rigid rotation with a velocity of  $\sim 300 \text{ km s}^{-1}$  (Sofue et al. 2001; Koda et al. 2002). This yields the velocity gradient of  $2.4 \text{ km s}^{-1} \text{ pc}^{-1}$ . Just as Baan & Irwin (1995) also Sawada-Satoh et al. (2000) have interpreted the equivalent HI components to originate against the two continuum components A and B, which in reality were components E and F (Middelberg et al. 2003). The velocity differences estimated from the CO velocity gradients between the two continuum components F (A) and E (B), separated by 25 mas or 2 pc, are only  $1.7 \text{ km s}^{-1}$  or  $4.8 \text{ km s}^{-1}$ . Such values are not consistent with the observed velocity difference of  $101.6 \text{ km s}^{-1}$  between OH1 and OH2, which would suggest that the two detected OH absorptions arise from neither the kpc-scale CO disk nor the nuclear CO core. MERLIN observations at  $\sim 400 \text{ mas}$  resolution resolved the rotational motion of the HI absorbing gas (Pedlar et al. 1996), which matches the sense of the rotation traced by the HI emission (Irwin & Seaquist 1991). The directions of the HI velocity fields in the three HI VLBI absorption components have not been presented in Sawada-Satoh et al. (2000), which prevents a comparison with the OH velocity fields in Fig. 5. Comparisons of the intensity distribution of OH1 and OH2 for each transition are presented in Fig. 6. The intensity maps were produced from the uniformly weighted spectral-line cubes. We find that there is a difference in the spatial

distribution in both 1667 MHz and 1665 MHz absorption, which is even more distinct in the 1665 MHz line. The distribution of the blue-shifted OH1 is downward w.r.t that of the systemic OH2 by approximately 8 mas, or 0.6 pc in declination. This trend is also true in the PV diagram of Fig. 3, where the difference is clearly seen for both main-lines.

## 4 DISCUSSION

### 4.1 The puzzle of the nuclear radio continuum

NGC 3079 is known to exhibit a complex radio structure in the nuclear region. Recent VLBI studies reveal a multiple milli-arcsec-scale nuclear source structure with five frequency dependent components (Middelberg et al. 2003). The continuum components A, B and C are only present in maps at 22 GHz but are totally obscured at L-band. The identification of a true nucleus in the galaxy has been a subject to debate. If the H<sub>2</sub>O maser structure is indeed confirmed to be a disk with a rotation axis misaligned by 15–20° with respect to the kpc-scale CO(1–0) disk at P.A.= 30°, then the nucleus would lie close to the A-C-B line (Fig. 7). Trotter et al. (1998) proposed that the dynamical center lies between components A and B, more specifically at the intersection of the jet axis and a north-south distribution of the H<sub>2</sub>O masers. The north-south distribution of the H<sub>2</sub>O maser was more convincingly confirmed in Kondratko (2003) by measuring the positions of the new red-shifted H<sub>2</sub>O maser features reported in Hagiwara et al. (2002a). An H<sub>2</sub>O disk centered close to C and having a systemic velocity of 1120 km s<sup>−1</sup> would be consistent with the H<sub>2</sub>O components at 1123 km s<sup>−1</sup> at C, the systemic velocity of the HI absorption of 1116 km s<sup>−1</sup>, and the systemic OH component (OH2) at 1114 km s<sup>−1</sup>. The models based on the velocity signature of the OH and HI absorption (Baan & Irwin 1995) and of the HI VLBI signature (Sawada-Satoh et al. 2000) refer to components E and F and do not reflect the location of the nucleus. Various monitoring programs have been executed to detect a velocity drift of the systemic components as seen in NGC 4258, but they have failed to find any drifting component to confirm the disk signature (e.g. Baan & Haschick 1996; Hagiwara et al. 2002a).

Considering the available evidence, the true nucleus is hidden at L-band and lies close to C on the line connecting components C and B. The nature of the L-band components E and F is not yet certain. These components could be circum-nuclear starburst regions but for that E has too high a brightness temperature and could be a supernova remnant.

### 4.2 The nature of the OH absorption

An important result of our EVN observations is the interpretation of the two different velocity fields traced by the two OH absorption components on scales of 10 mas towards the unresolved radio continuum nucleus. The spectrum in Fig. 1 shows that most of the OH absorption has been resolved out in our data set, as compared with single-dish and

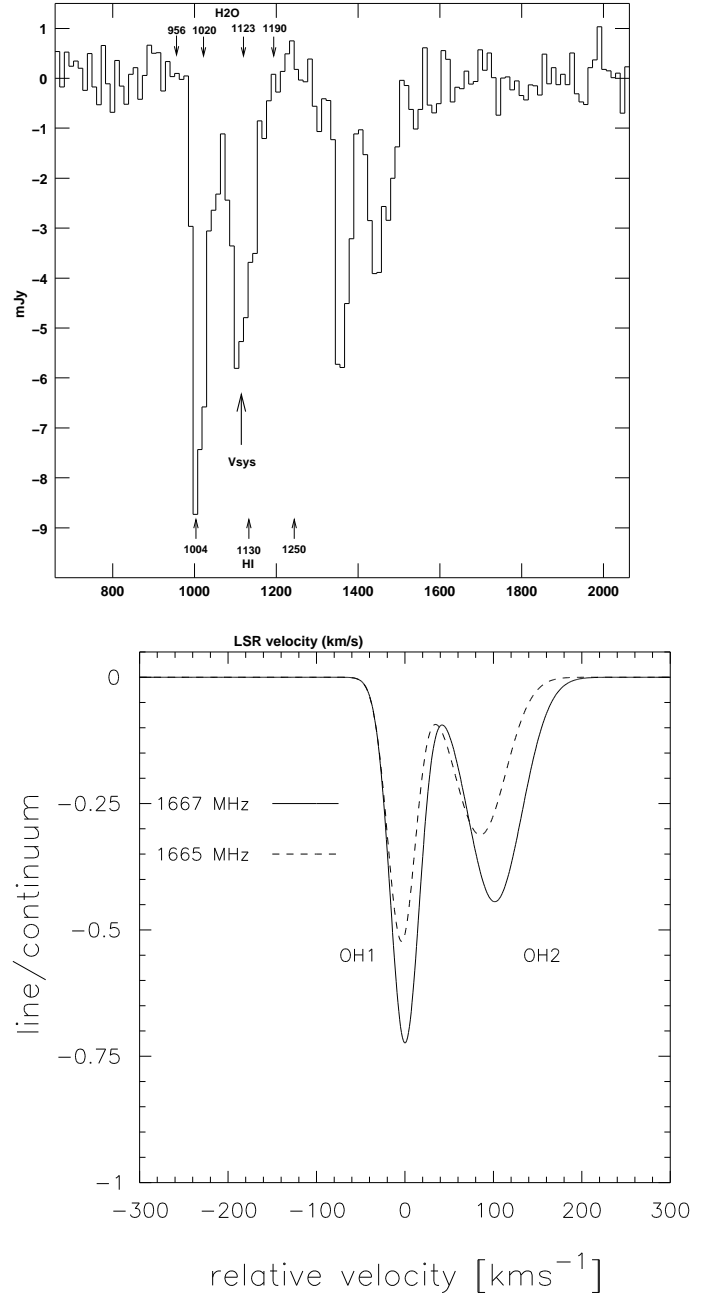


**Figure 1.** *left:* Hydroxyl absorption spectrum of the 1667 MHz and 1665 MHz transitions, obtained with the EVN in November 2000. An rms noise per channel is 0.7 mJy beam<sup>−1</sup>. The velocity resolution is 11.2 km s<sup>−1</sup>. Velocities in the spectra are scaled in the radio LSR convention. The adopted systemic velocity of NGC 3079 is  $V_{\text{LSR}} = 1116$  km s<sup>−1</sup>. The peak velocities of HI absorption and H<sub>2</sub>O maser are denoted by arrows. The results of 2-D Gaussian-fitting of the spectrum are listed in Table 1. *right:* Gaussian models fitted to the OH spectrum of the 1667 and 1665 MHz transition. The velocity is referenced to  $V_{\text{LSR}} = 1013$  km s<sup>−1</sup>, the Gaussian-fitted peak velocity of the 1667 MHz OH1 in Table 2.

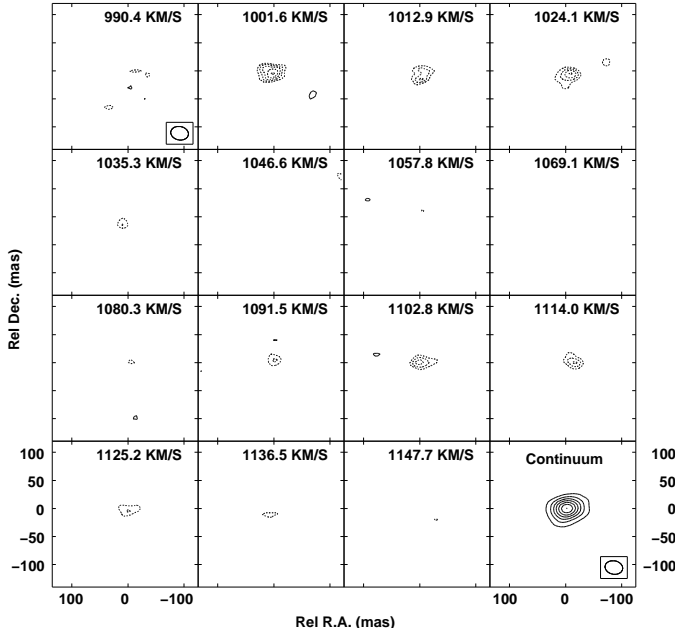


**Figure 2.** Velocity channel maps of uniformly weighted continuum-subtracted spectral line cube where the OH absorption at 1667 MHz is present. The contour levels are  $-8, -7, -6, -5, -4, -3, 3 \times 0.8 \text{ mJy beam}^{-1} (1 \sigma)$ . 18-cm uniformly weighted continuum map is also shown with the contour levels at  $-5, 5, 10, 15, 20, 25, 30, 35, 40 \times 0.25 \text{ mJy beam}^{-1} (1 \sigma)$ . The center  $(0,0)$  position is R.A.(J2000)= $10^h 01^m 57^s.805$  Dec.(J2000)= $+55^\circ 40' 47''.08$ . The synthesized beams are plotted at the top-left and the bottom-right corner.

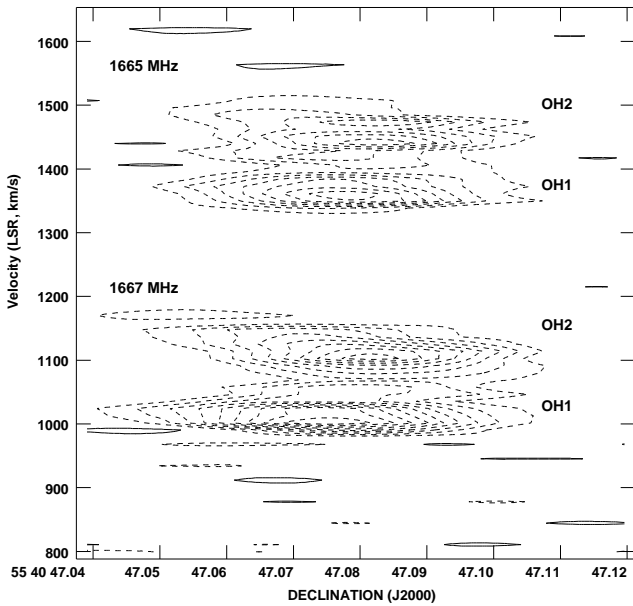


**Figure 3.** Position-velocity (PV) diagram produced from the naturally weighted spectral-line visibility cube, sliced along P.A.=  $15^\circ$  to align the major axis of the CO rotation (Sofue & Irwin 1992) and the cuts used in PV diagrams in (Baan & Irwin 1995). The contours are plotted at 10, 20, 30, 40, 50, 60, 70, 80, 90, 100 percent of the peak intensity of  $-6 \text{ mJy beam}^{-1}$ . The positive contour corresponds to  $+0.6 \text{ mJy beam}^{-1}$ .

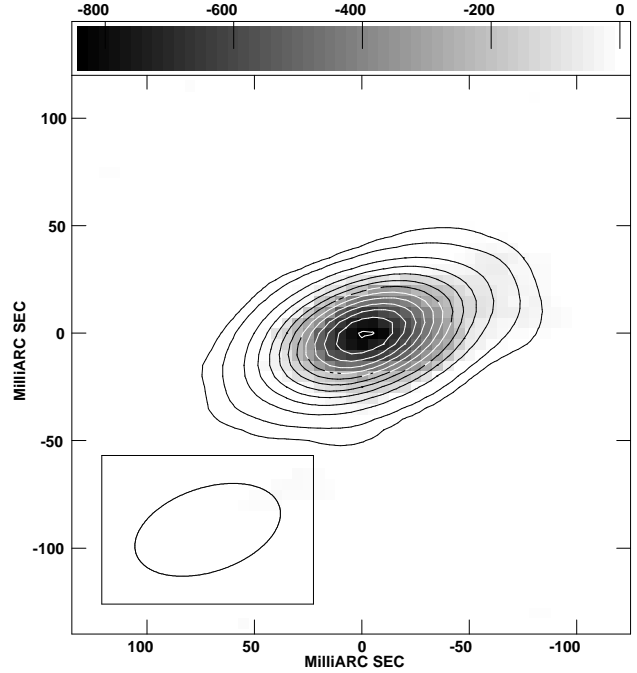


**Figure 4.** 18-cm naturally weighted continuum map (contour) superposed with a 1667 MHz OH intensity (0th moment) map (grey-scaled in  $\text{Jy beam}^{-1} \text{ m s}^{-1}$ ). The peak flux density of the continuum is  $10.3 \text{ mJy beam}^{-1}$ . The contours are plotted at  $-5, 5, 10, 20, 30, 40, 50, 60, 70, 80, 90, 100, 110, 120 \times 0.085 \text{ mJy beam}^{-1} (1 \sigma)$ . The synthesized beam ( $70 \text{ mas} \times 39 \text{ mas}$ , P.A.=  $-72^\circ$ ) is plotted on the lower left corner.

VLA spectra in Baan & Irwin (1995). This implies that we observe compact gas that extends no more than the beam size of 45 mas, or  $\sim 4 \text{ pc}$ , which is almost equal to the size of the background continuum. The OH absorbing gas has been interpreted primarily to be a part of circum-nuclear gas traced by the CO(1-0) emission (Baan & Irwin 1995). A single black body fit based on the measurement of far-infrared (FIR) flux densities at  $12 - 100 \mu\text{m}$  in NGC 3079 gives a temperature of 43 K and the maximum extent of this large-scale FIR source (e.g. torus) of about 130 pc. Our EVN data do not provide compelling evidence for such a large-scale torus.

#### 4.2.1 The absorbing gas structure

The nucleus of NGC 3079 hosts a LINER or a type 2 Seyfert nucleus. Therefore, the nucleus could be obscured by an edge-on dusty torus or intervening medium along the line of sight. Because of the systematic similarity of the HI and OH absorptions, Baan & Irwin (1995) suggested a possible association of the two HI and OH absorbing gas components with the double continuum source (Fig. 7). With a  $1.0 \text{ arcsec}$  (corresponding to  $80 \text{ pc}$ ) resolution of the VLA in A Configuration, the data in Baan & Irwin (1995) were insufficient to extract precise connections between these absorption components and the nuclear radio continuum structure.

Interpretation of the VLBI data in Sawada-Satoh et al. (2000) shows that the three HI components are resolved and that the column densities of each component against F

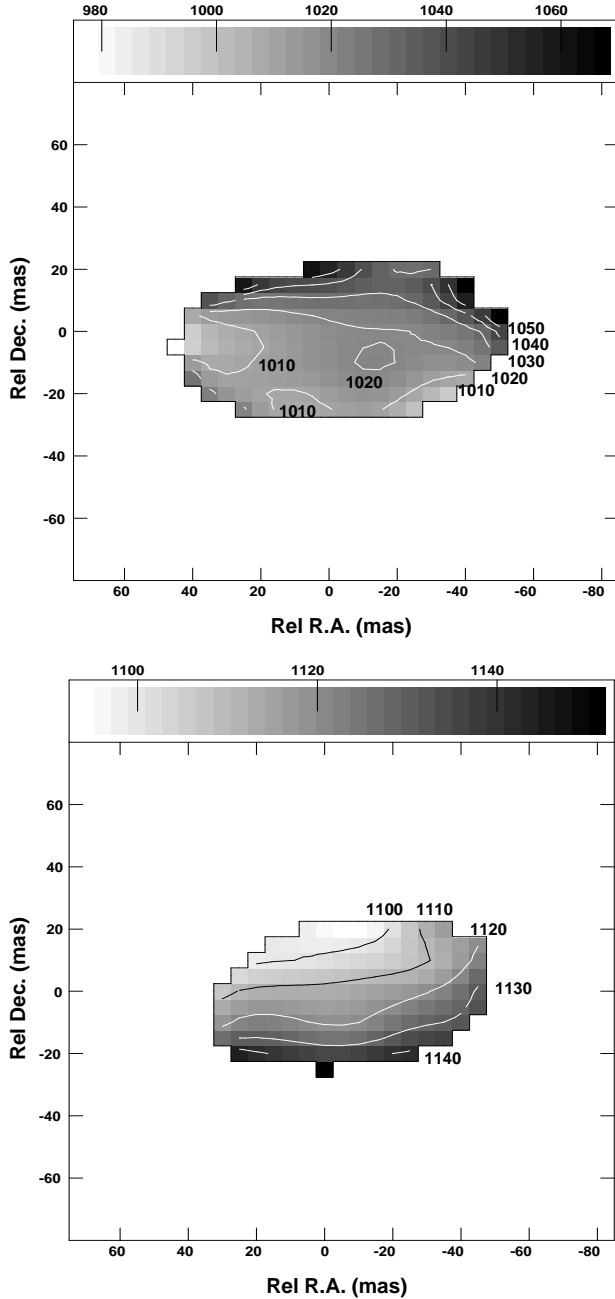


**Figure 5.** Mean velocity field (1st moment) of the two 1667 MHz OH absorption components. Contours are plotted every 10 km s<sup>-1</sup> in LSR velocities with the gray scales indicated on the top. *left*: blue-shifted component (OH1), *right*: systemic velocity component (OH2).

(blue-shifted HI), F+E (systemic HI), and E (red-shifted HI) are almost the same, suggesting that E and F are uniformly obscured by the ISM foreground to the nuclear sources. Our EVN data failed to resolve E from F, so that we cannot identify the individual contributions for OH absorption and the OH column densities for each component with those of HI. Baan & Irwin (1995) introduced a rotating disk model, in which the torus is confined in the roughly north-south orientation with an inclination about  $-20^\circ$  w.r.t the CO(1-0) disk standing at P.A. =  $15^\circ$ . In this discussion,

the jet axis connecting the nuclear radio sources of E and F makes an angle of about  $45^\circ$  with the confining torus. The sense of the rotation of the torus proposed in Baan & Irwin (1995) is consistent with that of the CO disk/core and the edge-on H<sub>2</sub>O maser disk proposed in Trotter et al. (1998) and Kondratko (2003). Sawada-Satoh et al. (2000) proposed a counter-rotating disk at P.A. =  $30^\circ$  in order to explain the spatially resolved HI absorption. However, the directions and position angles of the torus and the CO and H<sub>2</sub>O maser disks are completely inconsistent with those of the torus model in Sawada-Satoh et al. (2000) and the evidence for this counter-rotation is weak.

On the other hand, a counter-rotating structure reversed to the kiloparsec-scale CO(1-0) disk has been observed in OH absorption in a type 2 Seyfert galaxy NGC 5793 (Hagiwara et al. 2000). Similarly, two nuclear disks with radii  $\sim 100$  pc embedded in the outer kpc-scale gas disk have been clearly resolved in CO(2-1) in the merging nuclei of the ultra-luminous infrared galaxy Arp 220 (IC 4553). The rotational sense between these two disks is reversed due to the counter rotation of the two nuclei themselves (Sakamoto et al. 1999).

#### 4.2.2 Interpretations of the double OH peaks

The OH absorption in the EVN spectrum shows double peaks with a separation of 101.6 km s<sup>-1</sup> in velocity (Table 2). Baan & Irwin (1995) considered the association of OH1 and OH2 with the radio twin peaks E and F (Fig. 7) with an OH velocity gradient between the two components along the jet axis of approximately  $50 \cos \phi$  km s<sup>-1</sup> pc<sup>-1</sup>. The projected separation of the twin radio peaks E and F is  $\sim 25$  mas or 2 pc and the projected angle ( $\phi$ ) lies between the radio axis E-F and the plane of the OH gas motion. The value of the gradient would be 10 times larger than that of the CO(1-0) kpc-scale disk and the CO(1-0) nuclear core rotating in the north-south direction, unless  $\cos \phi$  is unrealistically small. Consequently, it is not plausible to correlate the OH velocity difference between E and F and the internal velocity gradients of the CO(1-0) disk/core, although the direction of the OH velocity gradients agrees with that of the larger-scale CO(1-0) disk. This velocity gradient would also be about 10 times larger than those seen in the merging galaxy Arp 220 (Mundell, Ferruit & Pedlar 2001) and the Seyfert galaxies Mrk 231 and Mrk 273 (Klöckner, Baan, & Garrett 2003; Klöckner & Baan 2003), where HI absorption or OH maser emission reveal a rotating molecular torus with an inner radius of several tens of parsecs from the central engine. Considering the available evidence, the double peaks must arise from two kinematically independent systems in the nuclear region. The direction of the velocity gradient of the systemic OH2 is in good agreement with that of the CO and H<sub>2</sub>O maser disks. In addition, the velocity range of OH2 nearly coincides with the systemic velocity of NGC 3079. We know that the HI absorption at the systemic velocity is seen against the whole nuclear continuum at 21-cm (Sawada-Satoh et al. 2000). This can be accounted for by clumpy gas in a kiloparsec-scale disk. Accordingly, the systemic OH2 probes gaseous components in the CO disk, and particularly the inner disk on scales of 10-100 pc. On the other hand, the velocity field of the blue-shifted

OH1 is very different from that of OH2 and of the CO disk. Baan & Irwin (1995) argued that a foreground and an expanding shell driven by the nuclear superbubble could explain the large blue-shift of the OH1 centroid velocity, while a receding shell may account for the other weak red-shifted OH absorption component around  $V_{\text{LSR}} = 1260 \text{ km s}^{-1}$ , as observed with VLA. In the starburst galaxy M82, distinct outflow components of molecular gas were discovered that extend over 500 pc above the plane of the disk and lie along the minor axis of the galaxy (e.g. Nakai et al. 1987).

It is uncertain whether or not the outflows traced by OH1 are associated with the (possible) starburst-related components E and F themselves because the velocity gradient of OH1 does not align with this E-F axis (Fig. 7). It should be noted that the velocity range of OH1 ( $V_{\text{LSR}} = 956\text{--}1050 \text{ km s}^{-1}$ ) overlaps with that of several blue-shifted H<sub>2</sub>O features peaking at velocities  $V_{\text{LSR}} = 1012, 1018, 1034$ , and  $1035 \text{ km s}^{-1}$  (Trotter et al. 1998). Although these features have a velocity signature similar to that of the OH1 absorption component, there is no evidence for a physical association. Some of the H<sub>2</sub>O maser components outside the edge-on masering disk of the Circinus galaxy are interpreted as molecular outflow components, ejected from the edge-on structure (Greenhill et al. 2003).

The two OH emission features identified at  $V_{\text{LSR}} = 910 \text{ km s}^{-1}$  and  $1230 \text{ km s}^{-1}$  in Baan & Irwin (1995) and detected weakly in our data may be accounted for by the blue-shifted 1667 MHz and 1665 MHz OH features that lie at velocities just below the OH1 outflow components. They may arise in the shocked molecular components foreground to the outflow structure. In the above picture, an association with molecular outflows can explain the blue-shifted OH1, the weak OH emission, and also possibly the H<sub>2</sub>O maser components. However, this last association cannot be quantified due to difficulties in comparing the distribution of weak H<sub>2</sub>O masers and the OH absorption on very different angular scales.

## 5 CONCLUSIONS AND SUMMARY

The broad OH absorption towards the nuclear continuum source in NGC 3079 was imaged using VLBI techniques. The EVN observations reveal two kinematically independent OH absorption components, where OH1 is the blue-shifted absorption, and OH2 is the absorption at the systemic velocity of the galaxy. The understanding of the kinematics of these components is limited by the fact that the 18-cm background continuum and the OH components have not been spatially resolved.

1. The OH2 component shows a distinct velocity gradient in roughly north-to-south direction viewed against the unresolved nuclear continuum at 18-cm consisting of components E and F. This velocity gradient of the systemic OH2 is consistent with that of the clumpy gas component in the kpc-scale CO disk (P.A. =  $15^\circ$ ).

2. The blue-shifted component OH1 appears to be associated with molecular outflows and is possibly associated with the nuclear super-bubble due to circum-nuclear starburst activity at components E and F and possibly at other locations. The velocity gradient of the OH1 component is not yet understood but is almost reversed from that of the

systemic component OH2. The weak OH emission features marginally detected in our EVN observation may also be associated with shocked gas in these nuclear outflows.

3. The H<sub>2</sub>O masers in the galaxy have been attributed to a compact disk structure around the true nucleus located west of the radio continuum component C. The OH1 velocity range is similar to that of the blue-shifted H<sub>2</sub>O maser components and there may be some relation.

The combined knowledge of our OH data, of previous VLBI data on the radio continuum, of H<sub>2</sub>O masers, and of the HI absorption on scales of 100 pc down to sub-parsec scales, provides a clear and consistent interpretation of the various spectral components seen at the nucleus. VLBI observations at even higher angular resolution and high sensitivity could resolve the nature of the OH and HI components in relation to H<sub>2</sub>O maser components in the nuclear region of NGC 3079.

## ACKNOWLEDGMENTS

This research has made use of the NASA/IPAC Extragalactic Database (NED), which is operated by the Jet Propulsion Laboratory, California Institute of Technology, under contract with the National Aeronautics and Space Administration. The European VLBI Network is a joint facility of European, Chinese, South African and other radio astronomy institutes funded by their national research councils. We thank the anonymous referee for useful comments.

## REFERENCES

- Baan W.A., 1989, *ApJ*, 338, 804
- Baan W.A., Irwin J.A., 1995, *ApJ*, 446, 602
- Baan W.A., Haschick A., 1996, *ApJ*, 473, 269
- Braatz J.A., Wilson A.S., Henkel C., 1996, *ApJS*, 106, 51
- Cecil G., Bland-Hawthorn J., Veilleux S., Filippenko A.V., 2001, *ApJ*, 555, 338
- Cecil G., Bland-Hawthorn J., Veilleux S., 2002, *ApJ*, 576, 745
- Condon J.J., 1983, *ApJS*, 53, 459
- Ford H.C., Dahari O., Jacoby G.H., Crane P.C., Ciardullo R., 1986, *ApJ*, 311, L7
- Greenhill L.J., Booth R.S., Ellingsen S.P., et al., 2003, *ApJ*, 590, 162
- Hagiwara Y., Diamond P.J., Nakai N., Kawabe, R., 2000, *A&A*, 360, 49
- Hagiwara Y., Henkel C., Sherwood W.A., Baan W.A., 2002a, *A&A*, 387, 29L
- Hagiwara Y., Henkel C., Sherwood W.A., 2002b, in *Migenes V., Reid M.J., eds, IAU Symp. 206, Cosmic Masers: From Protostars to Black Holes*, p.392
- Haschick A.D., Baan W.A., 1985, *Nature*, 314, 14
- Haschick A.D., Baan W.A., Schneps M.H., Reid M.J., Moran J.M., Güsten R., 1990, *ApJ*, 356, 149
- Heckman T.M., 1980, *A&A*, 87, 152
- Henkel C., Güsten R., Downes D., Thum C., Wilson T.L., Biermann P., 1984, *A&A*, 141, L1
- Herrnstein J.R., Greenhill L.J., Moran J.M., Diamond P.J., Inoue M., Nakai N., Miyoshi M., 1998, *ApJ*, 497, L69
- Irwin J.A., Seaquist E.R., 1988, *ApJ*, 335, 658

- Irwin J.A., Seaquist E.R., 1991, ApJ, 371, 111  
 Irwin J.A., Sofue Y., 1992, ApJ, 396, L75  
 Klöckner H-R, Baan W.A., Garrett M.A., 2003, Nature, 421, 821  
 Klöckner H-R, Baan W.A., 2004, A&A, in press  
 Koda J., Sofue Y., Kohno K., Nakanishi H., Onodera S., Okumura S.K., Irwin J.A., 2002, ApJ, 573, 105  
 Kondratko P. T., 2003, research exam paper, Harvard University  
 Middelberg E., Kurichbaum T.P., Roy A.L., Witzel A., Zensus J.A., 2003, in Romney J.D., Reid M.J., eds, Proc. Future Directions in High Resolution Astronomy: A Celebration of the 10th Anniversary of the VLB. Astron. Soc. Pac., San Francisco, in press  
 Mundell C.G., Ferruit P., Pedlar A., 2001, ApJ, 560, 168  
 Nakai N., Hayashi M., Handa T., Sofue Y., Hasegawa T., Sasaki M., 1987, PASJ, 39, 685  
 Pedlar A., Mundell C.G., Gallimore J.F., Baum S.A., O'Dea C.P., 1996, Vistas Astron., 40, 91  
 Sakamoto K., Scoville N.Z., Yun M.S., Crosas M., Genzel R., Tacconi L.J., 1999, ApJ, 514, 68  
 Sawada-Satoh S., Inoue M., Shibata K.M., Kamenno S., Migenes V., Nakai N., Diamond P.J., 2000, PASJ, 52, 421  
 Sawada-Satoh S., Inoue M., Shibata K.M., Kamenno S., Nakai N., Migenes V., Diamond P.J., 2001, in Schilizzi R.T., Vogel S.N., Paresce F., Elvis M.S., eds, Proc. IAU Symp. 205, Galaxies and their Constituents at the Highest Angular Resolutions, p.196  
 Sofue Y., Irwin J.A., 1992, PASJ, 44, 353  
 Sofue Y., Koda J., Kohno K., Okumura S.K., Honma M., Kawamura A., Irwin J.A., 2001, ApJ, 547, L115  
 Trotter A.S., Greenhill L.J., Moran J.M., Reid M.J., Irwin J.A., Lo K.-Y. 1998, ApJ, 495, 740

This paper has been typeset from a  $\text{\LaTeX}$  file prepared by the author.

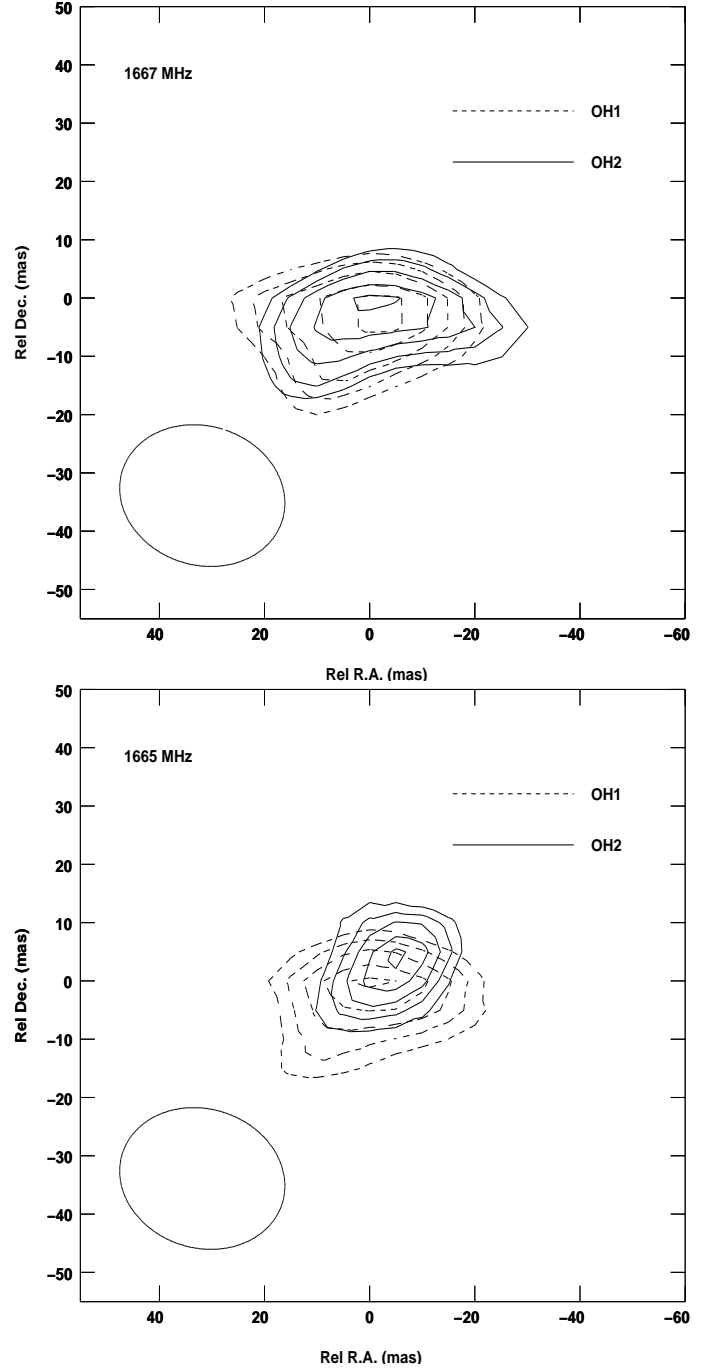


**Figure 6.** Comparison of the intensity distribution of the OH double peaks OH1 and OH2, integrated over 16 velocity channels (corresponding to  $\sim 180 \text{ km s}^{-1}$ ) for each peak. Contour levels run from -2 to -1.2 mJy per beam in steps of 0.2 mJy per beam. The synthesized beam is included at the left corner of each plot. *left:* 1667 MHz, *right:* 1665 MHz. The dashed and solid lines show OH1 (blue-shifted absorption) and OH2 (near systemic velocity), respectively.



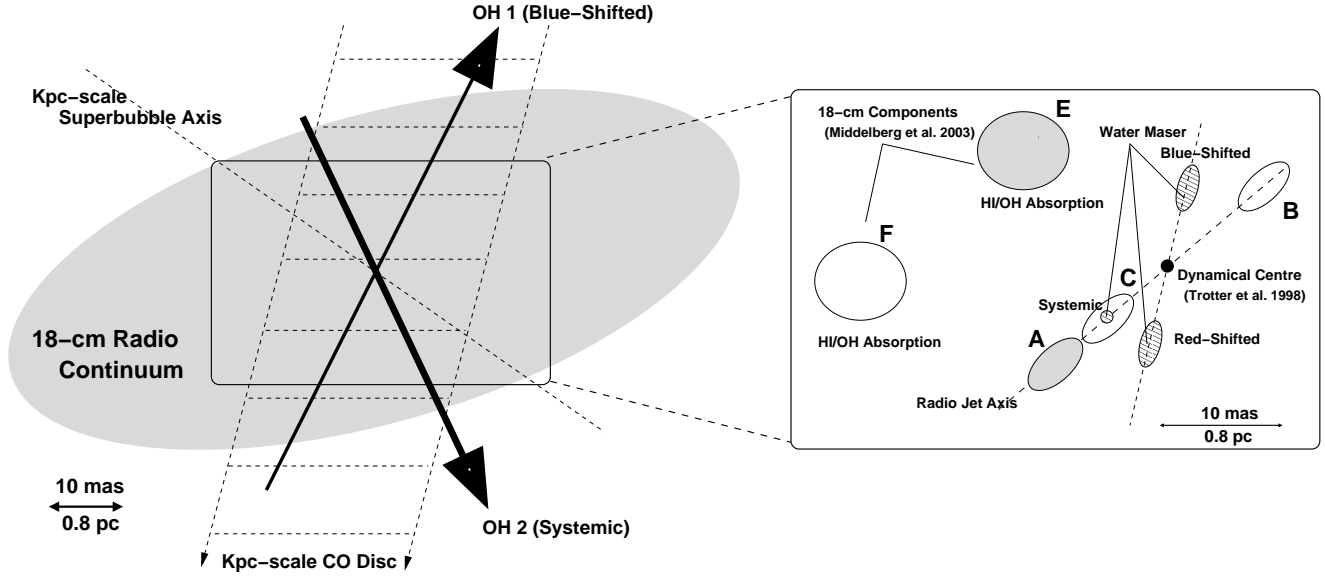


**Figure 7.** Schematic views of the nuclear region of NGC 3079. The sizes of components are drawn roughly in scale. Oval indicates the outline of the unresolved continuum nucleus in Fig. 2. Upward thin arrow denotes the direction of OH1 velocity gradient against E and F, both of them are not resolved in our EVN observations. Downward thick arrow shows the sense of the OH2 velocity gradient that is roughly consistent with the kpc-scale CO rotation, indicated by thin dashed arrows. A thin dashed line denotes the axis of the kiloparsec-scale super-bubble consisting of wide-angle outflows ejected from the nuclear region (Cecil et al. 2001). Inset displays the innermost nuclear region of NGC 3079, where three radio sources A, B, and C are aligned along P.A.= 55°. The weak component C may be shaded by the inclined torus or disk traced by the H<sub>2</sub>O masers (Trotter et al. 1998). Components E and F are visible at lower frequencies at from 1.7 to 5.0 GHz (Kondratko 2003; Middelberg et al. 2003) and may result from circum-nuclear starburst. The component labels are adopted from the nomenclature defined in Irwin & Seaquist (1988) and Middelberg et al. (2003). Components E and A show similar spectral characteristics, that are different from other components. The spectra of E and A are inverted at 2.3 and 5.0 GHz, respectively (Middelberg et al. 2003).

**Table 2.** Gaussian-fitted parameters of the OH absorption and emission spectra. VLA data are from Baan & Irwin (1995). Vc refers a line-peak velocity. Sp and  $\Delta V$  are peak flux density and linewidth (FWHM), respectively. The EVN measurements of the OH emission are tentative.

	VLA			EVN (This paper)		
	Vc (km s <sup>-1</sup> )	Sp (mJy beam <sup>-1</sup> )	$\Delta V$ (km s <sup>-1</sup> )	Vc (km s <sup>-1</sup> )	Sp (mJy beam <sup>-1</sup> )	$\Delta V$ (km s <sup>-1</sup> )
OH ABSORPTION						
OH1 (1667 MHz)	1013	22	84	1011.9 ± 0.9	8.5 ± 0.4	38.7 ± 2.2
(1665 MHz)	1354	15	-	1361.6 ± 1.3	6.1 ± 0.4	37.2 ± 3.1
OH2 (1667 MHz)	1114	27	92	1113.5 ± 2.0	5.2 ± 0.3	72.1 ± 5.0
(1665 MHz)	1462	18	-	1450.7 ± 2.9	3.6 ± 0.3	67.8 ± 7.3
OH EMISSION						
(1667 MHz)	910	4.7	61	(~900)	(0.5)	-
(1665 MHz)	1260	1.7	-	(~1235)	(0.5)	-

**Table 3.** Parameters of the 1667 MHz OH absorption. Global-VLBI data are from Sawada-Satoh et al. (2001) and VLA data are from Baan & Irwin (1995).

	EVN		Global-VLBI		VLA (A Configuration)	
	OH1 (Blue-shift)	OH2 (Systemic)	OH1	OH2	OH1	OH2
Optical depth ( $\tau$ )	0.46 ± 0.03	0.31 ± 0.02	0.73 ± 0.17	0.79 ± 0.13	1.03	1.28
N <sub>OH</sub> /T <sub>ex</sub> (K <sup>-1</sup> cm <sup>-2</sup> )	4.3 × 10 <sup>15</sup>	5.3 × 10 <sup>15</sup>	9.2 × 10 <sup>16</sup>	1.8 × 10 <sup>17</sup>	2.2 × 10 <sup>16</sup>	2.5 × 10 <sup>16</sup>